A Spectroscopic Study of Colchicine in the Solid State and in Solution by Multinuclear Magnetic Resonance and Vibrational Circular Dichroism

by **Albert Virgili***[a]), **Mª Mar Quesada-Moreno**[b]), **Juan Ramón Avilés-Moreno**[b]), **Juan Jesús López-González***[b]), **M. Ángeles García**[c]), **Rosa M. Claramunt***[c]), **M. Rosario Torres**[d]), **M. Luisa Jimeno**[e]), **Felipe Reviriego**[e]), **Ibon Alkorta***[e]), and **José Elguero**[e])

[a]) Departament de Química, Universitat Autònoma de Barcelona, Bellaterra, E-08193 Cerdanyola, Barcelona (e-mail: albert.virgili@uab.es)

[b]) Department of Physical and Analytical Chemistry, University of Jaén, Campus Las Lagunillas, E-23071 Jaén (e-mail: jjlopez@ujaen.es)

[c]) Departamento de Química Orgánica y Bio-Orgánica, Facultad de Ciencias, Universidad Nacional de Educación a Distancia (UNED), Senda del Rey 9, E-28040 Madrid

[d]) CAI de Difracción de Rayos-X, Facultad de Ciencias Químicas, Universidad Complutense de Madrid (UCM), E-28040 Madrid

[e]) Instituto de Química Médica (CSIC), Juan de la Cierva, 3, E-28006 Madrid (e-mail: ibon@iqm.csic.es)

Dedicated to *Artur Bladé-Font* for his contributions to the chemistry of colchicinoids

Although almost 200-years-old, several unknown aspects remain to be explored of colchicine, the unique available drug for acute flares of gout. In this article, we report density-functional theory (DFT) studies of geometry, energy, and NMR; ^{1}H-, ^{13}C-, and ^{15}N-NMR chemical shifts and some spin-spin coupling constants, including the complete analysis of the saturated part (ring *B*); the assignment of both enantiomers by NMR using a chiral solvating agent; solid-state NMR experiments of the different forms of natural and racemic colchicine, and IR and vibrational circular dichroism (VCD) studies of these same forms.

1. Introduction. – Colchicine (**1**), first isolated in 1820 by *Pelletier* and *Caventou* from *Colchicum autumnale*, is still the main agent for treatment of acute cases of gout. As inhibitor of microtubule polymerization by binding to tubulin, it is continually used, with a remarkable history, as an experimental tool for characterizing the biochemical properties of tubulin, the protein subunit of microtubules, for characterizing the diverse processes in eukaryotic cells that are dependent upon drug-sensitive microtubules, and for studying the polymerization and dynamics properties of microtubules. Recently, colchicine has been the focus of numerous investigations as a potential anticancer drug [1–4].

Its historical importance is also apparent when the names of scientists related to colchicine are listed: *Michael J. S. Dewar*, *Lynn Margulis*, *Albert Eschenmoser*, *Eugene E. van Tamelen*, *David A. Evans*, *Robert B. Woodward*, Sir *James W. Cook*, *Paul Knochel*, *Kyriacos C. Nicolaou*, *etc.*

The natural product is the (−)-colchicine [5][6], and the racemic compound, (±)-colchicine, was prepared by *Bladé-Font* in 1977 [7][8]. Mutarotation was never observed with colchicine, and the stereogenic C-atom C(7) contributes modestly to the

circular dichroism (CD) of colchicinoids, which is mainly determined by the helicity along the chirality axis C(12a)–C(12b) [9][10].

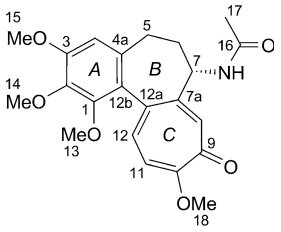

1

The structural information about colchicine is abundant, for instance, its ^{13}C-NMR spectrum has been recorded several times (*Table 1*) since our first report in 1979 [11].

Several X-ray structures of colchicine have been reported [16], starting from that of *King* in 1952 (a clathrate of the natural product) [6]: (−)-colchicine · 2 H_2O (COLCDH

Table 1. *^{13}C-NMR Chemical Shifts of* **1** *Determined in $CDCl_3$*[a]). Arbitrary atom numbering indicated in the formula of **1**.

Position	Reference/spectrometer frequency [MHz]					This work		GIAO (gas)
	[11]/20	[12][b])/20	[13][c])/15	[14]/90	[15]/100	125 MHz	150 MHz	
1	150.7	150.7	153.8*	151.0	151.1	150.88	151.20	153.0
2	141.1	141.1		141.4	141.6	141.33	141.67	145.1
3	153.2	153.2	151.4*	153.4	153.5	153.30	153.58	154.4
4	108.0	108.0		107.3	107.4	107.09	107.36	103.0
4a	134.4	134.4		134.3	134.2	134.11	134.25	135.2
5	29.4	29.4		29.8	29.8	29.66	29.91	32.8
6	36.0	36.0		36.1	52.7*	35.97	36.70	40.9
7	51.7	51.7		52.9	52.7	52.64	52.59	52.7
7a	151.2	151.2		153.0	152.6	152.77	152.44	150.4
8	134.7*	130.7	130.7	130.0	130.4	130.12	130.56	132.4
9	178.4	178.4		179.4	179.6	179.27	179.18	173.1
10	163.8	163.8		163.9	164.0	163.78	164.03	166.0
11	112.3	112.3		113.1	112.9	112.89	113.05	106.7
12	130.7*	134.7	134.7	135.8	135.5	135.54	135.79	136.7
12a	135.6	135.6		137.1	137.0	136.92	137.06	135.9
12b	125.7	125.7		125.5	125.6	125.34	125.56	130.0
13	60.9	60.9		61.5	61.4	61.34	61.60	59.2
14	60.7	60.7		61.3	61.2	61.15	61.44	57.6
15	55.9	55.9		56.1	56.1	56.26	56.49	52.4
16	168.9	168.9		170.2	170.0	170.05	169.90	169.3
17	22.4	22.4		22.6	22.6	22.42	22.95	21.8
18	56.0	56.0		56.5	56.3	55.90	56.14	52.8
^{15}N	–	–	–	–	–	– 256.1	–	–258.0

[a]) The wrong assignments are marked with asterisk (*). [b]) In 1980 [12], we modified the assignment of C(8) and C(12). [c]) The assignment of C(8) and C(12) was corrected, but the authors made an error in assigning C(1) and C(3) [11].

and COLCDH01, these structures have no H-atoms located) [6][17], (−)-colchicine · 1 H_2O (PALYOQ) [18], and (±)-colchicine · 2 H_2O (DOTMOO) [8].

However, several aspects have never been studied: ^{1}H-NMR analysis of the saturated part (CH_2(5)–CH_2(6)–CH(7)–NH); theoretical calculations of the geometry and NMR properties; the use of chiral reagents to determine if it is possible to differentiate both enantiomers by NMR; the use of solid-state NMR to compare the different colchicines (natural *vs.* racemic, anhydrous *vs.* H_2O solvates); as well as the possible application of solid-state vibrational circular dichroism (VCD) to identify the different colchicines. Herein, we report our results concerning these different aspects, which needed the confirmation by X-ray crystallography of the three reported structures, COLCDH, PALYOQ, and DOTMOO.

2. Results and Discussion. – 2.1. *DFT Theoretical Calculations at the B3LYP/6–311++G(d,p) Level.* Colchicine can exists in two diastereoisomers, (R_a,7*S*) and (S_a,7S), and their interconversion results in mutarotation (*Fig. 1*) [10], the (R_a,7*S*)-diastereoisomer being the most stable (13–15 kJ mol^{-1} depending on the theoretical method used). On the other hand, boat–boat interconversion of methoxytropolone ring *C* results in two atropisomers, that on the left side being the most stable (*ca.* 13 kJ mol^{-1}) [19][20].

The geometry we minimized, starting from one of the X-ray structures of (−)-**1**, corresponds to the (R_a,7*S*) diastereoisomer and to the most stable atropisomer (dihedral angle in both cases *ca.* 53°). This structure was used for the NMR calculations (δ and *J*; *cf. Sect. 2.2.1*), and for the IR and VCD calculations (*Sect. 2.3*).

Colchicine racemization concerns the amide group at C(7) (*Scheme*) from the natural colchicine, (7*S*), to the other enantiomer, (7*R*), this being accompanied by the (R_a) → S_a enantiomerization.

Scheme. *Enantiomerization of Colchicine*

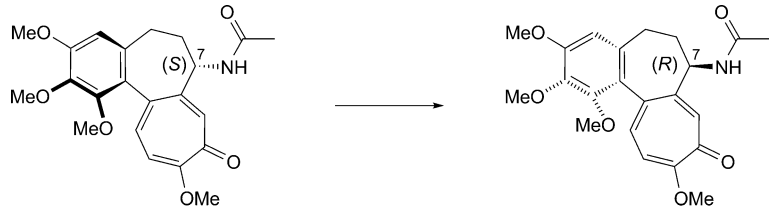

(R_a,7*S*)-**1** (S_a,7*R*)-**1**

2.2. *NMR Studies.* 2.2.1. *NMR Solution Studies. Determination of the Conformation of the Saturated Part of Ring* B *by ^{1}H-NMR.* In *Fig. 2*, the calculated ^{1}H-NMR chemical shifts of colchicine (for the Me groups, the three H-atoms have been averaged) as well as those measured in $CDCl_3$ are shown.

Using the data in *Fig. 2*, *Eqn. 1* is obtained:

$$\text{Exp. } CDCl_3 = (1.070 \pm 0.015)\ \text{calc. GIAO},\ n = 14,\ R^2 = 0.998,$$
$$\text{worse points, H–C(11) } (+0.42\ \text{ppm}) \text{ and } H_a\text{–C(5) } (-0.40\ \text{ppm}). \qquad (1)$$

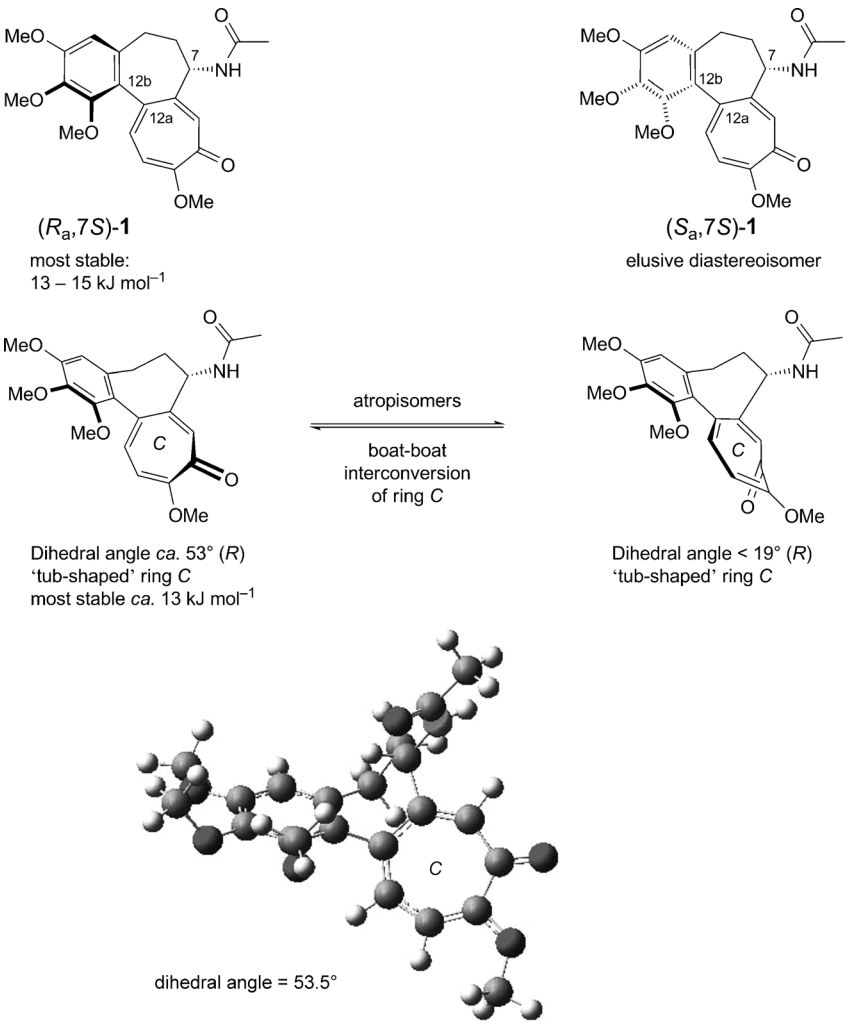

Fig. 1. *Consequences of the rotation about the C(12)–C(12b) bond and boat-boat interconversion of ring* C

Concerning the saturated part and the relationship of ^3J(H,H) vicinal coupling constants with dihedral angles, the main results are compiled in *Table 2*.

The B3LYP/6-311++G(d,p) calculated spin-spin coupling constants (SSCCs) are in good agreement with those determined by analysis of the spectrum in $CDCl_3$. The part concerning the vicinal coupling constants is of interest, because they are related to the conformation of the seven-membered ring *B*. For this subset, the agreement is still good between experimental and B3LYP values. The dihedral angles ϕ corresponding to the conformation of minimum energy can be transformed to vicinal coupling constants by means of one of the *Karplus*-type relationships. For the H–C–C–H fragments, we have selected the *Haasnoot–Altona* equation [21], and for the H–C–N–H fragment,

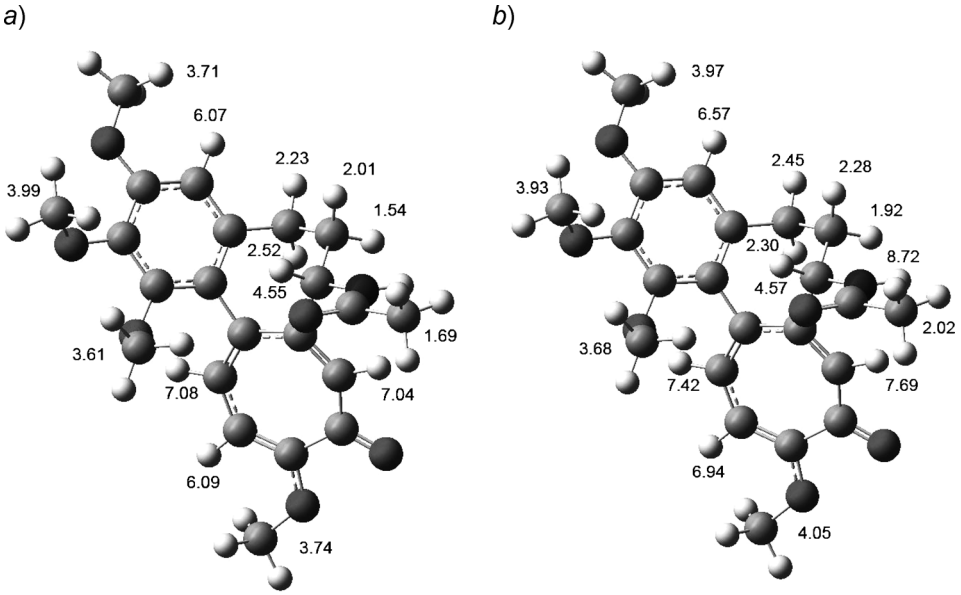

Fig. 2. *^{1}H-NMR Chemical shifts. a*) GIAO on the calculated geometry of minimum energy; the calculated value of the NH H-atom is not given. *b*) Experimental values in $CDCl_3$.

the *Ludvigsen* equation [22][23]. The closer to experimental values are those B3LYP calculated:

Note that the calculated minimum-energy conformation usually differs from the average conformation at the temperature of the experiment. Our results, i.e., *Eqn. 2*, show that this difference appears to be not very important.

$$^3J(\mathrm{H,H})\ \text{exp.}\ [\mathrm{Hz}] = (1.03 \pm 0.06)\ ^3J(\mathrm{H,H})\ \text{calc.}\ [\mathrm{Hz}],\ n = 7,\ R^2 = 0.976 \qquad (2)$$

2.2.2. *NMR Solution Studies. Differentiation of Enantiomers in the Presence of Chiral Solvating Agents.* Full NMR assignments are available as *Supplementary Material* from one of the corresponding authors (*A. V.*); nevertheless in *Fig. 3* the assignments of the H-atoms of the Me groups through an HMBC experiment are illustrated.

The comparison of the ^{13}C-NMR data obtained at 150 MHz with the GIAO calculated values (*Table 1*) affords the following *Eqn. 3:*

$$^{13}\mathrm{C}\ (\text{exp.})\ [\mathrm{ppm}] = (1.003 \pm 0.006)\ ^{13}\mathrm{C}\ (\mathrm{GIAO})\ [\mathrm{ppm}],\ n = 22,\ R^2 = 0.9993 \qquad (3)$$

Including the ^{15}NH (determined at 125 MHz), *Eqn. 4* is obtained.

$$^{13}\mathrm{C},^{15}\mathrm{N}\ (\text{exp.})\ [\mathrm{ppm}] = (0.998 \pm 0.006)\ ^{13}\mathrm{C},^{15}\mathrm{N}\ (\mathrm{GIAO})\ [\mathrm{ppm}],\ n = 23,\ R^2 = 0.9993 \qquad (4)$$

A series of experiments were carried out both by ^{1}H- and by ^{13}C-NMR to determine if the enantiomers could be differentiated and, if so, assigned. To this aim, we have

Table 2. *Coupling Constants of the Saturated Fragment of Ring* B ($CH_2(5)$–$CH_2(6)$–CH(7)–NH). SSCC, Spin-spin coupling constant.

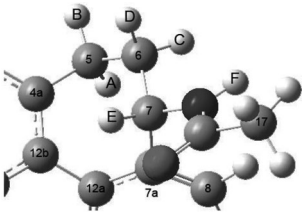

Experimental (concentrated solutions, $\geq$50 mg/0.6 ml) δ [ppm]: 2.30 (A), 2.45 (B), 1.92 (C), 2.28 (D), 4.57 (E) 8.72 (F)					
Experimental SSCC [Hz]:					
J(A,B) = −13.8					
J(A,C) = 7.3	J(B,C) = 1.0				
J(A,D) = 12.7	J(B,D) = 8.3	J(C,D) = −13.5			
J(A,E) = 0.0	J(B,E) = 0.0	J(C,E) = 12.2	J(D,E) = 6.0		
J(A,F) = 0.0	J(B,F) = 0.0	J(C,F) = 0.0	J(E,F) = 6.1		
SSCC [Hz] Directly calculated (corresponding to the minimum-energy conformation)					
J(A,B) = −12.1					
J(A,C) = 6.7	J(B,C) = 1.1				
J(A,D) = 11.3	J(B,D) = 6.3	J(C,D) = −10.6			
J(A,E) = −0.3	J(B,E) = −0.6	J(C,E) = 10.2	J(D,E) = 6.2		
J(A,F) = 0.0	J(B,F) = 0.0	J(C,F) = 0.0	J(E,F) = 6.1		
^3J(H,H) Vicinal					
SSCC	Exp.	B3LYP	Dihedral	ϕ [°]	*Karplus*
J(A,C)	*7.3*	*6.6*	ϕ_{AC}	*43.7*	*6.7*
J(A,D)	12.7	13.4	ϕ_{AD}	161.3	11.3
J(B,C)	1.0	0.9	ϕ_{BC}	−72.6	1.1
J(B,D)	8.3	6.3	ϕ_{BD}	45.0	6.3
J(C,E)	12.2	10.2	ϕ_{CE}	168.0	14.2
J(D,E)	6.0	6.2	ϕ_{DE}	51.3	4.8
J(E,F)	6.1	7.9 (NH)	ϕ_{EF}	−153.3	8.0 (NH)

prepared and used a chiral solvating agent (CSA) that has proved very efficient in previous studies, (*S*,*S*)-ABTE (=α,α'-bis(trifluoromethyl)anthracene-9,10-dimethanol) [24–26].

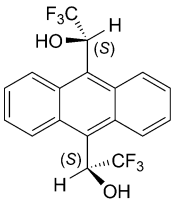

(*S*,*S*)-ABTE

In *Table 3*, the ^{1}H- and ^{13}C-NMR results are completed.

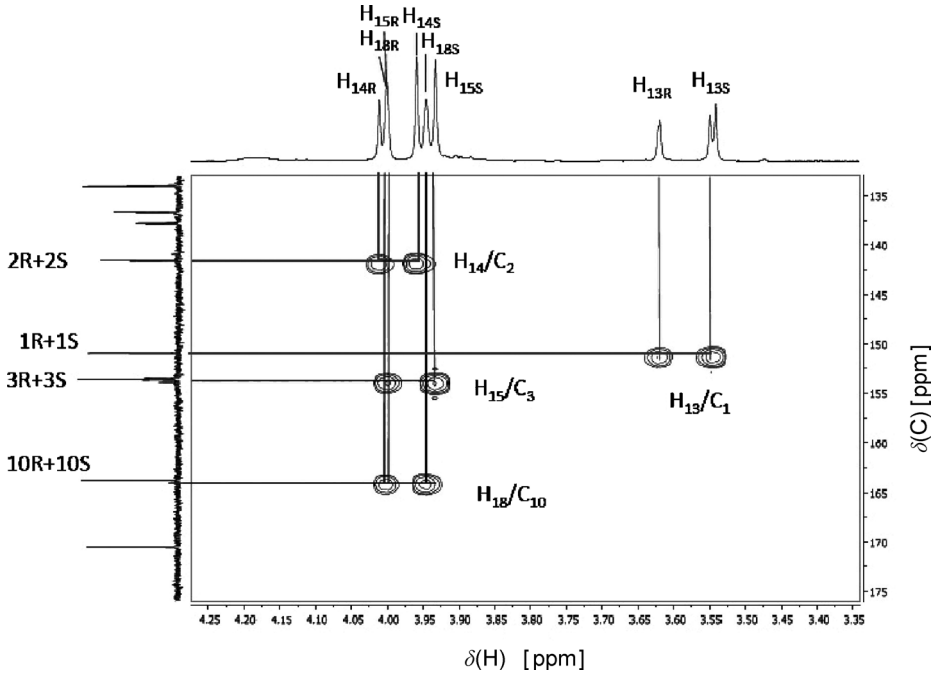

Fig. 3. *HMBC Experiment*

In bold, we have indicated the signals with largest $\Delta\Delta\delta$ that are useful to assign the absolute configuration at C(7). The NH H-atom (F) shows the largest effect (0.64 ppm) but it is too sensitive to concentration effects to be used when only one enantiomer is present. It has been reported that the NH H-atoms are very sensitive to the concentration when the used solvent is $CDCl_3$ [27]. The ^{15}N-NMR signal is very sensitive to the absolute configuration, but it is more difficult to record than either ^{1}H- or ^{13}C-NMR.

The effects observed on the ^{13}C-NMR chemical shifts led us to propose the formation of diastereoisomeric complexes (*Fig. 4*) between each enantiomer of colchicine, the (−) or natural, and the (+), and (*S*,*S*)-ABTE. That from the (−)-colchicine has been optimized using *Truhlar M05-2X* functional appropriate for weak intermolecular interactions [28]. The results (*Fig. 4*) indicate that one of the OH groups of (*S*,*S*)-ABTE forms a H-bond with the C=O of the colchicine (tropolone ring *C*). The Me(17) group of the amide at C(7) is close to one of the aromatic rings of ABTE. We calculated its chemical shifts [GIAO/B3LYP/6-311++G(d,p)] on the optimized M05–2X geometries: the effects (δ (complex) – δ (colchicine)) are −0.64 ppm for ^{1}H and −0.73 ppm for ^{13}C, that compare well with the respective values in *Table 3*, −0.40 and −0.87 ppm.

2.2.3. *Solid-State CPMAS-NMR Experiments.* In principle, there are five possible samples (−)-**1** (anh.), (−)-**1**·H_2O (PALYOQ), (−)-**1**·2 H_2O (COLCDH), (±)-**1** (anh.), and (±)-**1**·2 H_2O (DOTMOO), but only four have been obtained (*Table 4*).

Table 3. *Enantiodifferentation of* (7S)- (natural, (−)) *and* (7R)-*Colchicines in the Presence of* (S,S)-*ABTE* (all values in ppm). $\Delta\Delta\delta$ is (7*R*−7*S*) or $\Delta\delta_{7R}-\Delta\delta_{7S}$. Very diluted solution.

H-Atom	δ_{rac}	δ_S	δ_R	$\Delta\delta_{S-rac}$	$\Delta\delta_{R-rac}$	$\Delta\Delta\delta_{R-S}$
H–C(4)	6.57	6.50	6.53	−0.07	−0.04	0.03
H_A–C(5)	2.33	1.98	1.76	−0.35	−0.57	**−0.22**
H_B–C(5)	2.41	2.11	2.11	−0.30	−0.30	0.00
H_C–C(6)	1.95	1.42	1.51	−0.44	−0.53	−0.09
H_D–C(6)	2.57	2.34	2.34	−0.23	−0.23	0.00
H–C(7)	4.69	4.17	3.82	−0.52	−0.87	**−0.35**
H–C(8)	7.69	7.26	7.13	−0.43	−0.56	−0.13
H–C(11)	6.94	6.85	6.90	−0.09	−0.04	0.05
H–C(12)	7.42	7.35	7.32	−0.07	−0.10	−0.03
Me(13)	3.68	3.52	3.63	−0.16	−0.05	0.11
Me(14)	3.93	3.96	4.02	0.03	0.09	0.06
Me(15)	3.97	3.94	4.03	−0.03	0.06	0.09
Me(17)	2.02	1.38	0.97	−0.64	−1.05	**−0.41**
Me(18)	4.05	3.95	4.02	−0.10	−0.03	0.07
NH[a])	7.45	7.21	7.85	−0.24	0.40	**0.64**
Atom	δ_{rac}	δ_S	δ_R	$\Delta\delta_{S-rac}$	$\Delta\delta_{R-rac}$	$\Delta\Delta\delta_{R-S}$
C(1)	151.20	151.40	151.43	0.20	0.23	0.03
C(2)	141.67	141.91	142.00	0.24	0.33	0.09
C(3)	153.58	154.00	154.41	0.42	0.83	**0.41**
C(4)	107.36	107.86	108.54	0.50	1.18	**0.68**
C(4a)	134.25	134.39	134.31	0.14	0.06	−0.08
C(5)	29.91	29.92	29.92	0.01	0.01	0.00
C(6)	36.70	36.45	35.86	−0.25	−0.84	**−0.59**
C(7)	52.59	53.04	52.93	0.45	0.34	−0.11
C(7a)	152.44	153.68	154.00	1.24	1.56	0.32
C(8)	130.56	129.85	129.32	−0.71	−1.24	**−0.53**
C(9)	179.18	179.40	179.30	0.22	0.12	−0.10
C(10)	164.03	164.20	164.20	0.17	0.17	0.00
C(11)	113.05	114.25	114.48	1.20	1.43	0.23
C(12)	135.79	136.97	137.20	1.18	1.41	0.23
C(12a)	137.06	137.98	138.27	0.92	1.21	0.29
C(12b)	125.56	125.49	125.37	−0.07	−0.19	−0.12
Me(13)	61.60	61.96	62.10	0.36	0.50	0.14
Me(14)	61.44	61.84	61.92	0.40	0.48	0.08
Me(15)	56.49	56.73	56.64	0.24	0.15	−0.09
C(16) = O	169.90	171.06	170.95	1.16	1.05	−0.11
Me(17)	22.95	22.22	21.55	−0.73	−1.40	**−0.67**
Me(18)	56.14	56.75	56.75	0.61	0.61	0.00
^{15}NH	−256.8	−254.6	−255.7	2.2	1.1	**−1.1**

[a]) The NH signal is concentration-dependent. In concentrated solutions (50 mg/0.6 ml), it appears at 8.72 ppm (*Table 2*), while, in diluted solutions (6 mg/0.6 ml), it appears at 7.45 ppm.

Crystals of (−)-**1**·H_2O (PALYOQ) were too small to undergo diffraction, and, accordingly, this structure was abandoned.

According to the data in *Table 4*, the spectra of (−)-**1** (anh.) and that of (±)-**1** (anh.) are very similar, but this does not take into account the multiplicity both in ^{13}C- and in

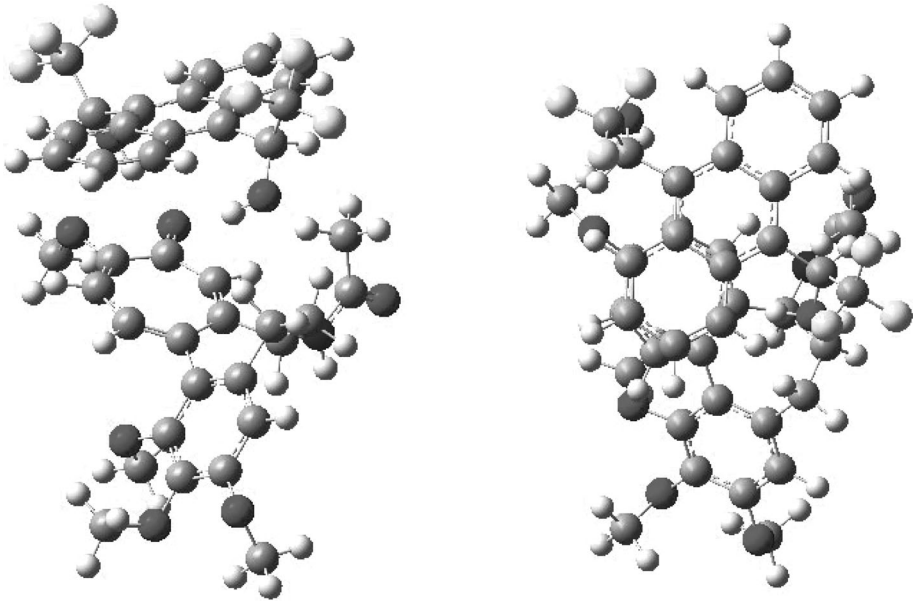

Fig. 4. *Two views of the complex formed by (−)-colchicine and (*S,S*)-ABTE. Left*, lateral view; *right*, top view.

^{15}N-NMR (*Fig. 5*). The anhydrous form (amorphous) of (−)-**1** is a complex mixture of structures, (see, *e.g.*, the four major peaks in ^{15}N-CPMAS-NMR (*Fig. 5*, *bottom*) at −249.3, −251.9, −252.9 (less intense), and −254.2 ppm). The spectrum corresponding to COLCDH is very well resolved, and almost all C-atoms and the N-atom appear as two signals, one for each independent molecule in the unit cell.

We calculated the chemical shifts for each one of the independent molecules maintaining the non located H-atoms in the positions determined by X-ray crystallography (remember that COLCDH structure has no located H-atoms [17]) and optimizing the positions of the H-atoms. If we assign the order (larger/smaller) of the experimental values to the order calculated for molecule A and molecule B, we obtain the values listed in *Table 5*. We have already used this approach in other cases with success [29].

Since the ^{15}N signal is very far apart from the ^{13}C signals, we have carried out the comparisons with and without it:

$$\mathrm{a} = (0.99 \pm 0.01)\ \mathrm{A},\ n = 23,\ R^2 = 0.997; \tag{5}$$

without ^{15}N, $\mathrm{a} = (1.009 \pm 0.008)\ \mathrm{A},\ n = 22,\ R^2 = 0.9985$ (6)

$$\mathrm{b} = (1.008 \pm 0.008)\ \mathrm{B},\ n = 23,\ R^2 = 0.9987; \tag{7}$$

without ^{15}N, $\mathrm{b} = (1.018 \pm 0.007)\ \mathrm{B},\ n = 22,\ R^2 = 0.9990$ (8)

2.3. *IR and VCD Studies.* Although, in some rare cases, it is possible to determine the absolute configuration of a molecule devoid of heavy atoms by X-ray crystallog-

Table 4. *^{13}C-NMR Chemical Shifts of* **1** *Determined in the Solid State* (CPMAS[a])) *at 100 MHz*

Atom	(−)-**1**[b]) (anh.)	(−)-**1**·2 H_2O (COLCDH)	(±)-**1** (anh.)	(±)-**1**·2 H_2O (DOTMOO)
C(1)	151.2	149.9, 149.9	151.7	152.7
C(2)	141.0	140.5, 141.6	140.7	141.5
C(3)	153.3	153.9, 156.7	154.0	154.1
C(4)	107.2	106.6, 107.8	107.9	107.5
C(4a)	134.9	134.8, 134.8	134.7	134.2
C(5)	28.9	28.8, 30.8	30.2	30.8
C(6)	36.4	35.4, 37.4	37.5	35.8
C(7)	55.8	55.1, 55.7	54.9	54.1
C(7a)	153.0	151.4, 153.0	151.7	153.5
C(8)	130.1	129.5, 130.1	132.6	131.5
C(9)	178.7	177.6, 179.9	179.7	178.9
C(10)	164.5	163.0, 164.5	164.7	164.5
C(11)	113.8	113.0, 116.3	113.1	112.6
C(12)	137.4	137.6, 138.5	136.9	136.7
C(12a)	135.5	134.8, 134.8	135.5	134.9
C(12b)	126.0	125.0, 125.8	126.1	126.0
Me(13)	61.7	61.9, 61.9	63.0	61.2
Me(14)	58.4	59.3, 60.5	60.6	60.3
Me(15)	53.8	52.0, 53.4	51.5	53.0
C(16) = O	170.5	169.8, 170.8	169.7	170.0
Me(17)	20.3	21.8, 22.4	23.7	21.9
Me(18)	55.8	56.1, 57.8	54.9	57.9
^{15}N	−252.5	−244.3, −249.5	−246.6	−254.6

[a]) CPMAS, Cross-polarization magic angle spinning. [b]) Almost every signal is split (2 or 3 lines), the values correspond to an average.

raphy [30], the application of the *Bijvoet* method (anomalous scattering) [31] usually requires the presence of a heavy atom such as Br. In recent years, the use of solid-state VCD has offered the possibility to determine the absolute configuration of compounds that are chiral in the solid state as well as in solution. The method involves the comparison of the theoretical VCD spectra of the expected configuration in the solid and liquid states with the experimental VCD spectra obtained under the above-mentioned conditions. The case of conformers (*R*,*S*) is much simpler than that of helices (*M*,*P*) [32], because it is sufficent to calculate the structure of the monomer. In this work, we analyzed the IR, *Raman*, and VCD spectra of four samples of colchicine: (−)-**1** (anh.), (−)-**1**·2 H_2O (COLCDH), (±)-**1** (anh.), and (±)-**1**·2 H_2O (DOTMOO). As mentioned in *Sect. 2.2.3*, crystals of PALYOQ were too small to diffract, and this structure was abandoned.

Interpretation of the VCD-spectral features of medium-size chiral compounds is a difficult task [33]. Our experience has revealed that a previous vibrational analysis for them, from IR and *Raman* data, and quantum-chemical calculations, is a convenient approach. Also, the availability of experimental and theoretical VCD data could be helpful for this aim and, then for a better knowledge of the absolute configuration in chiral molecules [34].

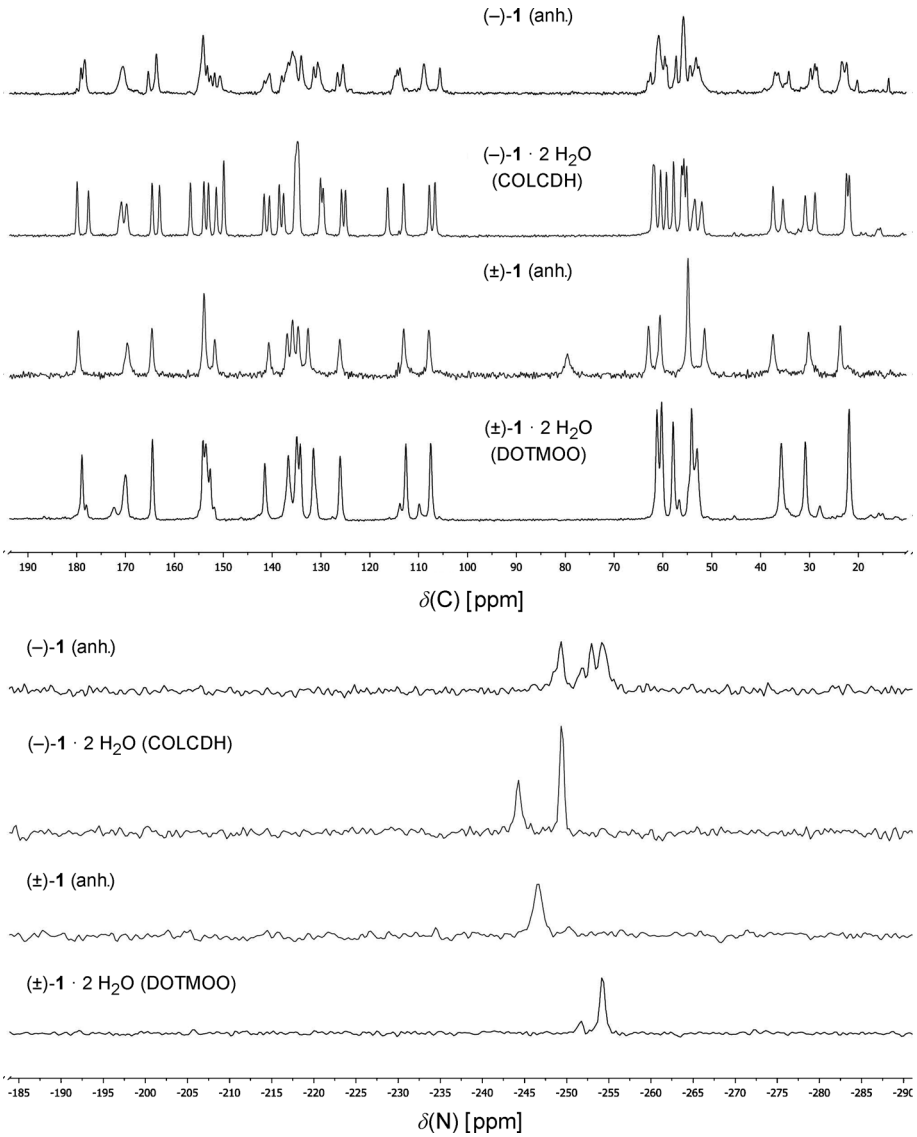

Fig. 5. *^{13}C- and ^{15}N-CPMAS spectra* (*top* and *bottom*, resp.) *of the four colchicines of* Table 4.

Thus, *i*) we recorded the IR and *Raman* spectra of the four samples of colchicine in $CHCl_3$ solutions and nujol/fluorolube mulls; *ii*) we compared them with the calculated B3LYP/6-311++G(d,p) spectra of the four structures after applying a frequency scale factor of 0.965 [35]. The scaled theoretical IR, *Raman*, and VCD spectra are in good agreement with the experimental spectra obtained in the solid and $CHCl_3$ solutions.

Table 5. *^{13}C-NMR Chemical Shifts of COLCDH Theoretically Calculated for Molecules A and B and Determined in the Solid State* (*Table 3*)

Atom	A	B	a	b
C(1)	148.51	147.61	149.9	149.9
C(2)	145.45	138.87	141.6	140.5
C(3)	158.35	153.34	156.7	153.9
C(4)	103.15	107.52	106.6	107.8
C(4a)	132.16	138.87	134.8	134.8
C(5)	31.08	30.97	30.8	28.8
C(6)	42.22	39.87	37.4	35.4
C(7)	50.56	56.99	55.1	55.7
C(7a)	146.17	146.09	153.0	151.4
C(8)	128.38	129.59	129.5	130.1
C(9)	180.88	175.43	179.9	177.6
C(10)	166.12	161.19	164.5	163.0
C(11)	107.10	103.27	116.3	113.0
C(12)	134.66	136.28	137.6	138.5
C(12a)	136.13	140.36	134.8	134.8
C(12b)	125.15	125.51	125.0	125.8
Me(13)	54.64	58.36	61.9	61.9
Me(14)	57.99	56.79	60.5	59.3
Me(15)	51.30	54.27	52.0	53.4
C(16) = O	156.39	164.74	169.8	170.8
Me(17)	21.20	21.24	21.8	22.4
Me(18)	55.21	54.02	57.8	56.1
^{15}N	– 266.84	– 258.61	– 249.5	–244.3

2.3.1. *Vibrational Spectra*. For clarity, the vibrational assignment is discussed by dividing the complete IR spectral range into several zones. For the discussion below, we comment the most relevant features which help to understand the vibrational spectrum of this molecule. The four analyzed samples, *i.e.*, (−)-**1** (anh.), (−)-**1**·2 H_2O (COLCDH), (±)-**1** (anh.), and (±)-**1**·2 H_2O (DOTMOO), have comparable IR and *Raman* spectra, indicating that a similar structure is found in the $CHCl_3$ solutions and mulls experiments (see *Figs. 6* and *7*).

In this work, DFT calculations were performed in the harmonic approximation. In this approach, overtones and combination bands were not taken into account. Thus, some bands appearing in the recorded IR and *Raman* spectra in the different regions studied are not predicted here.

In the N–H and C–H stretching region, some bands could be assigned to different normal modes, because there is a great overlapping (*Fig. 6*,*a*). The experimental bands observed around 3036 cm^{-1} (*Raman*) and 3000 cm^{-1} (*Raman*) are assigned to the C–H stretching of the two aromatic rings. Additionally, the experimental bands observed around 2861 cm^{-1} (*Raman*) and 2838 cm^{-1} (*Raman*) were assigned to the C–H stretching of the Me and CH_2 groups.

The analysis of the spectral zone from 2000 to 700 cm^{-1} provides more information (*Fig. 6*,*b*–*d*). Additionally, the four samples of colchicine displayed similar IR and *Raman* features in the solid samples (*Raman*), $CHCl_3$ solution and nujol/fluorolube mulls (IR), *i.e.*, the most stable diastereoisomer (R_a,7*S*)-**1** was present. For example,

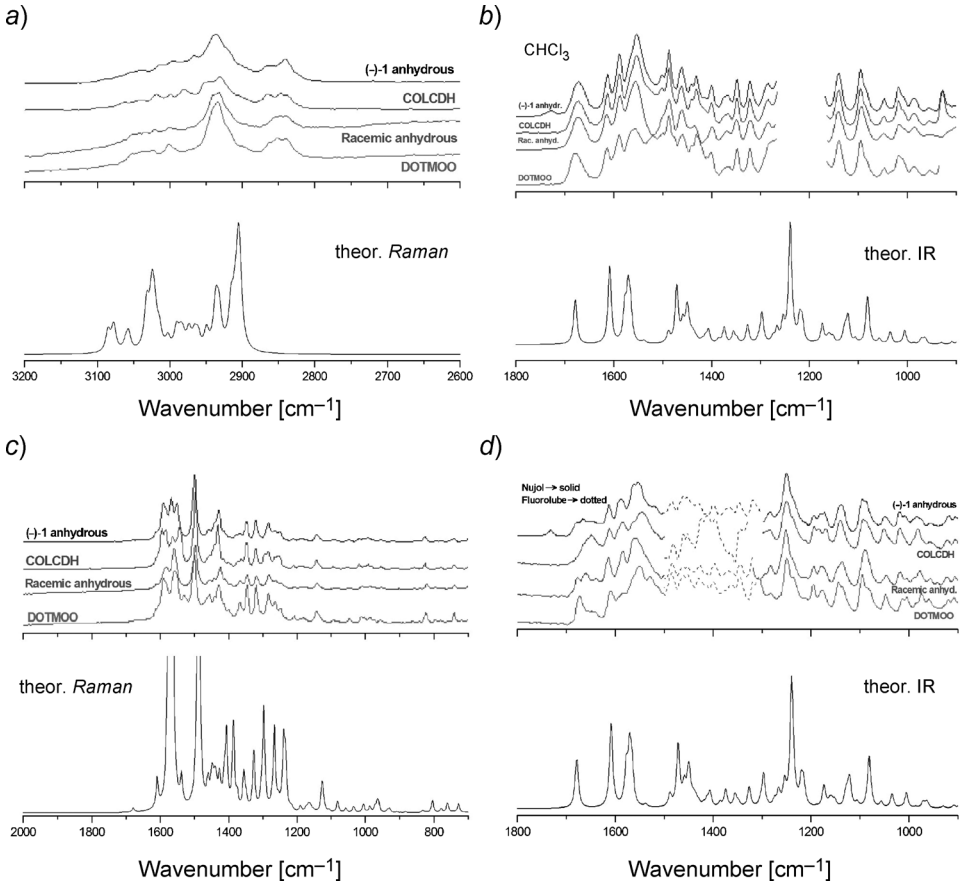

Fig. 6. *Experimental and scaled predicted* Raman (*a* and *c*) *and IR* (panels *b* and *d*) *spectra of the four samples of colchicine in the 3200–700-* (only for *Raman*) *and in the 1800–900-cm*$^{-1}$ (for IR) *spectral regions.* Experimental *Raman* spectra *a*) and *c*) for the solid samples of the four colchicines analyzed in this work. Experimental IR spectra for the $CHCl_3$ solutions (*b*) and solid samples (*d*) . In all cases, bottom panels show the scaled predicted *Raman* (*a* and *c*) and IR (*b* and *d*) spectra; NIST frequency scaling factor, 0.965; *Lorentzian* function, pitch, 1 cm^{-1}, FWHM (full width half maximum), 8 cm^{-1}.

the band observed at 1679 cm^{-1} (IR) was assigned to the C=O stretching of the amide group. The bands observed at 1588 (IR; 1592 cm^{-1} in *Raman*), 1570 (*Raman*), 1555 (IR; 1552 cm^{-1} in *Raman*), and 1500 cm^{-1} (IR; 1502 cm^{-1} in *Raman*) could be assigned to a mixed normal mode containing the C=O stretching of the C=O group in the seven-membered ring, and the C=C stretchings of the six- and seven-membered rings. Furthermore, the experimental bands observed at 1321 (IR; 1322 cm^{-1} in *Raman*), 1283 (IR; 1285 cm^{-1} in *Raman*), 1262 (*Raman*), and 1250 cm^{-1} (*Raman*) could be assigned to the CH_2 and Me waggings, and C–O stretchings. In addition, other interesting bands in this region were found at 1141 (IR; 1145 cm^{-1} in *Raman*) and 828 cm^{-1} (*Raman*), and they were assigned to the Me and CH waggings.

The low-frequency region, below 700 cm^{-1}, offered more detailed information for the vibrational analysis than the mid-IR region. It should be mentioned that the farIR and *Raman* data (*Fig. 7*) of the four samples were similar in both, solution and solid states, but (−)-**1** · 2 H_2O (COLCDH) presents a more intense far-IR spectrum than the other three samples, especially in the region below 150 cm^{-1}. This region shows normal modes with contributions of waggings, rockings, deformations, and torsions, *e.g.*, the experimental bands observed at 676 (IR; 679 cm^{-1} *Raman*) and 664 cm^{-1} (IR; 662 cm^{-1} *Raman*), which correspond to the six- and seven-membered rings deformations. Furthermore, the bands at 482 (IR; 484 cm^{-1} *Raman*), 453 (IR; 439 cm^{-1} *Raman*), and 437 cm^{-1} (IR; 439 cm^{-1} *Raman*) can be assigned to the N–H wagging, and six- and seven-membered rings deformations. Other examples are the bands observed at 236 (IR) and at 220 cm^{-1} (IR; 222 cm^{-1} *Raman*), which were assigned to the Me torsions.

Finally, since colchicine has substituent groups such as Me and MeO, it is possible to find some bands belonging to the torsions of these groups in the region below 300 cm^{-1}. For example, the bands found at 162 (IR; 156 cm^{-1} *Raman*), 94 (IR; 100 cm^{-1} *Raman*), and 65 cm^{-1} (IR) can be assigned to normal torsion modes of the Me and MeO moieties.

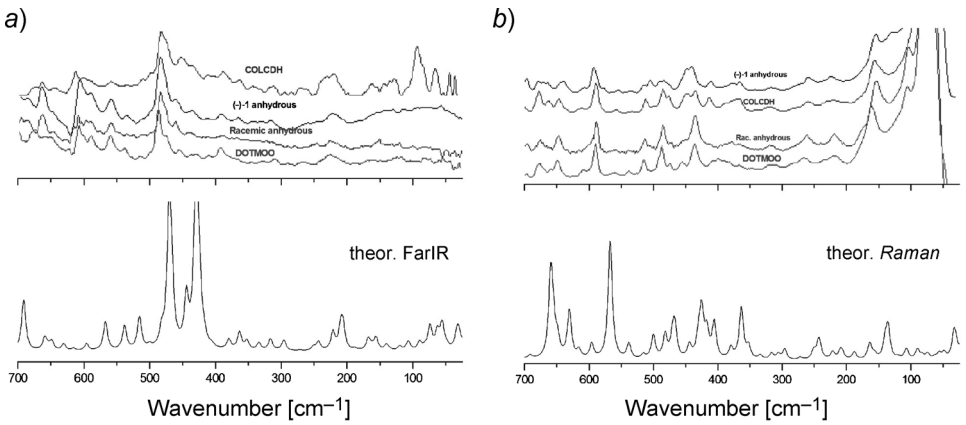

Fig. 7. *Experimental and scaled predicted Far-IR* (*a*) *and Raman* (*b*) *spectra of the four samples of colchicines in the 700–25-cm*$^{-1}$ *spectral region. Top:* Experimental far-IR spectra (*a*) and experimental *Raman* spectrum (*b*) of the solid. In both cases, bottom panels show the scaled predicted IR (*a*) and *Raman* (*b*); NIST frequency scaling factor, 0.965; *Lorentzian* function, pitch, 1 cm^{-1}, FWHM, 8 cm^{-1}.

2.3.2. *Vibrational Circular Dichroism* (*VCD*) *Spectra*. The VCD spectroscopy is a useful technique to deduce the absolute configuration of the structure (conformation and configuration) of colchicine. We analyzed the VCD spectra of four samples of colchicine, *i.e.*, (−)-**1** (anh.), (−)-**1** · 2 H_2O (COLCDH), (±)-**1** (anh.), and (±)-**1** · 2 H_2O (DOTMOO) in $CHCl_3$ solutions and fluorolube/nujol mulls. It was expected that only the two chiral samples, (−)-**1** (anh.) and (−)-**1** · 2 H_2O (COLCDH), presented a chirooptical response, *i.e.*, VCD features in solution or solid states. The signs of the rotatory strength could be helpful to determine the absolute configuration. Addition-

ally, we have successfully compared them with the calculated B3LYP/6-311++G(d,p) VCD spectra.

We observed a fair agreement between the experimental VCD spectra (in $CHCl_3$ solution and in fluorolube/nujol mulls) and the predicted scaled ones for the two chiral samples of colchicine (*Figs. 8* and *9*). The two racemic samples, (±)-**1** (anh.) and (±)-**1**·2 H_2O (DOTMOO), displayed a chirooptical response when the solution or mulls VCD spectra were recorded. *Figs. 8* and *9* display the experimental (in $CHCl_3$ solution and in fluorolube/nujol mulls) and theoretical VCD spectra of the four samples of colchicines in the 2000 – 900-cm^{-1} spectral region. A few experimental VCD bands evidence the presence of the chiral (−)-**1** in the liquid and solid phases.

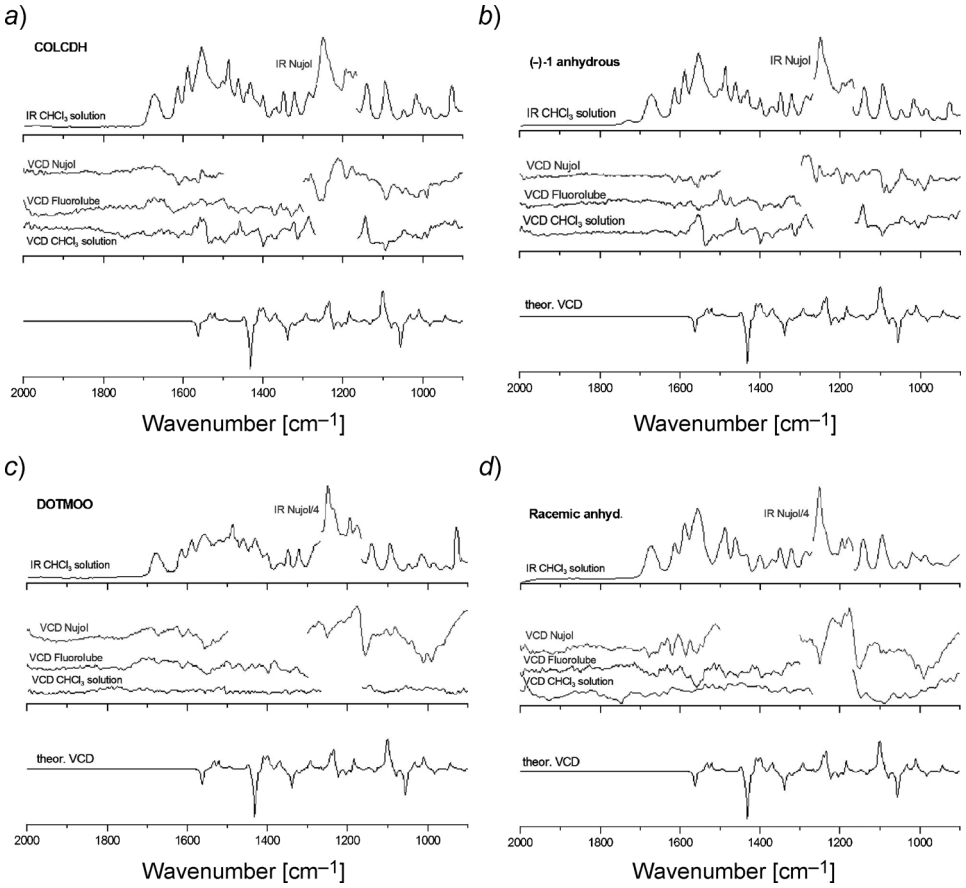

Fig. 8. *Experimental and theoretical VCD spectra of the four samples of colchicine in the 2000 – 900-cm^{-1} spectral region. a*) (−)-**1**·2 H_2O (COLCDH); *b*) (−)-**1** (anh.); *c*) (±)-**1**·2 H_2O (DOTMOO); and *d*) racemic (anh.). In all cases, bottom panels show the scaled predicted VCD spectrum, middle panels show the experimental VCD spectra in $CHCl_3$ solutions and nujol/fluorolube mulls, and top panels show the experimental IR spectra in $CHCl_3$ solutions and nujol mulls; NIST frequency scaling factor, 0.965; *Lorentzian* function, pitch, 1 cm^{-1}, FWHM, 8 cm^{-1}.

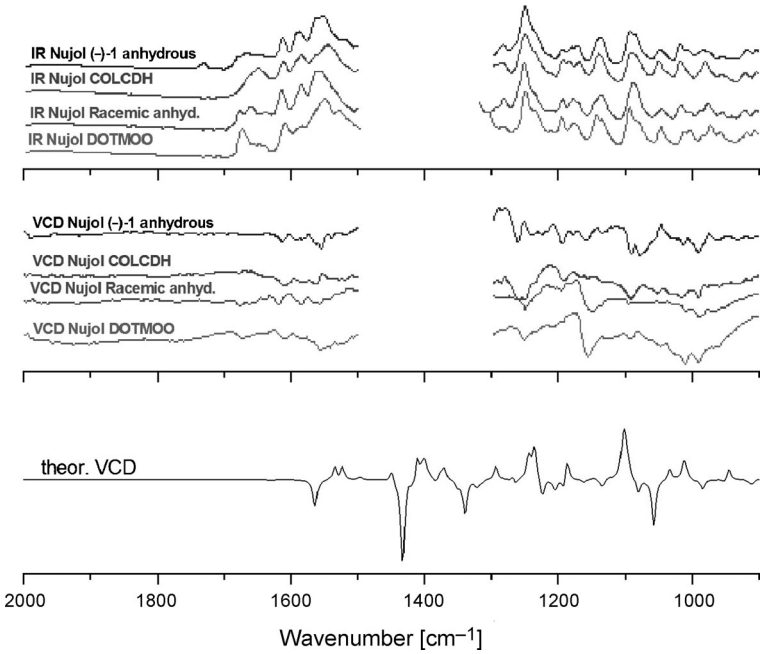

Fig. 9. *Experimental and theoretical VCD spectra of the four samples of colchicine in the 2000–900-cm^{-1} spectral region.* Bottom panels show the scaled predicted VCD spectrum, middle panels show the experimental VCD spectra in nujol/fluorolube mulls and top panels show the experimental IR spectra in nujol mulls; NIST frequency scaling factor, 0.965; *Lorentzian* function, pitch, 1 cm^{-1}, FWHM, 8 cm^{-1}.

The experimental VCD spectra of the two chiral samples in solution and mull were similar. This finding evidences the presence of the same chiral structure in both cases, *i.e.*, that of the most stable diastereoisomer (R_a,7*S*)-**1**.

First, we will comment the most relevant features of the VCD spectra in $CHCl_3$ solution and fluorolube/nujol mulls. The three (−, +, +) bands at 1537, 1512, and 1500 cm^{-1} (see *Sect. 2.3.1* for assignments) are well predicted by the presence of the most stable diastereoisomer (R_a,7*S*)-**1** in both solution and solid phases. In the same way, the two (−, +) bands at 1314 and 1285 cm^{-1} confirm the presence of the (R_a,7*S*)-**1** structure. Finally, other interesting bands are the (+, −) bands at 1144 and 1094 cm^{-1}, corresponding to the same structure. Similar conclusions were drawn from the analysis of the fluorolube/nujol mulls spectra of the two chiral structures of the colchicine molecule (*Figs. 8* and *9*). In both cases, the VCD spectra of the solid sample were in good agreement with the VCD features displayed by the solution experiments, *i.e.*, the chiral structures found in the solid and liquid phases are similar.

Furthermore, the two achiral samples, (±)-**1** (anh.) and (±)-**1** · 2 H_2O (DOTMOO), do not display chirooptical response in $CHCl_3$ solution, as expected. However, the two racemic samples present a weak chirooptical response in the solid phase (mulls spectra), which is weaker than the VCD features exhibited by the two chiral samples. This fact could be explained by a small enantiomeric excess of the minor configuration,

because the sign and position of the VCD bands indicate the presence of the minor enantiomer.

In conclusion, the chiral response of the two chiral samples is in good agreement with the presence of the most stable diastereoisomer (R_a,7*S*)-**1** in both, solution and solid spectra.

3. Conclusions. – This study of the important and irreplaceable colchicine provided some significant conclusions:

i) The natural (−)-colchicine ((−)-**1**) is the (R_a,7*S*) diastereoisomer, which is by 13 – 15 kJ mol^{-1} more stable than the (S_a,7*S*)-diastereoisomer.

ii) The conformation of the central ring *B* has been determined in solution by ^{1}H-NMR together with a combination of theoretical methods *i.e.*, B3LYP/6-311++G(d,p), and the *Karplus* equation.

iii) In the presence of (*S*,*S*)-ABTE, a chiral solvating agent, both enantiomers, (−)-**1** and (+)-**1** of (±)-**1** exhibit different NMR signals (^{1}H, ^{13}C, and ^{15}N). The structure of the complex that explains the observed effects has been validated by theoretical calculations.

iv) In the solid state, several known X-ray structures as well as amorphous forms have been studied by ^{13}C- and ^{15}N-CPMAS-NMR spectroscopy. The agreement, in terms of multiplicities, was satisfactory.

v) The IR and *Raman* spectra of four samples of colchicine (two racemic and two (−)-samples) were recorded in solution as well as in the solid state, and all bands, excluding overtones and combinations, were assigned based on scaled B3LYP/6-311++G** calculations. Eventually, we compared the VCD spectra recorded in $CHCl_3$ and nujol/fluorolube mulls with those calculated for the four samples studied in this work. That comparison allowed the determination of the absolute configuration of colchicine crystals as well as its configuration in solution.

With the technique in hand, it should be possible to determine the configuration of a specific sample of colchicine, *i.e.*, the main relation between its configuration and function.

This work was supported by the *Junta de Andalucía* (Project P08-FQM-04096). *M. M. Q. M.* thanks the University of Jaén for a predoctoral fellowship. Authors thank the University of Jaén for continuing financial support and its *CICT* for instrumental facilities. Authors also thank the *Ministerio de Economía y Competitividad* (CTQ2010-16122 and CTQ2012-35513-C2-02) and the *Comunidad Autónoma de Madrid* (Project MADRISOLAR2, Ref. S2009/PPQ-1533) for continuing support. Thanks are due to the *CTI* (*CSIC*) and to the *CESGA* for the allocation of computer time. We thank the Servei de Ressonància Magnètica Nuclear, Universitat Autònoma de Barcelona, for allocating instrument time. The help of Dr. Lourdes Infantes (Departamento de Cristalografía y Biología Estructural, Instituto de Química-Física *Rocasolano*, *CSIC*) with the facilities of the *CSD* is greatly acknowledged.

Experimental Part

1. *Racemization and Crystals.* The racemization of colchicine *N*-(= [(7*S*)-(5,6,7,9-tetrahydro-1,2,3,10-tetramethoxy-9-oxobenzo[*a*]heptalen-7-yl]acetamide), was carried out as described by *Bladé-Font* [7][8]. Both the natural and the racemic colchicines were dried under vacuum at 70°.

Crystals of natural colchicine were obtained from aq. soln. containing *Trizma* (=2-amino-2-(hydroxymethyl)propane-1,3-diol) · HCl buffer soln. (pH 7.4), m.p. 153 – 155° (no m.p. reported for

COLCDH [17]). Crystals of racemic colchicine were obtained from AcOH/H_2O, m.p. 291.6–292.7° ([6]: 282°) (DOTMOO).

2. *X-Ray Crystallography.* Data collection to determine the unit cell of a single crystal of each type was carried out at r.t. on a *Bruker Smart CCD* diffractometer using graphite-monochromated MoK_α radiation ($\lambda = 0.71073$ Å) operating at 50 kV and 30 mA.

The structure of COLCDH has been determined anew, and all crystallographic data were deposited with the *Cambridge Crystallographic Data Centre* with No. CCDC-924231. Formula $C_{44}H_{56}N_2O_{15}$, unit cell parameters: $a = 13.863(6)$ Å, $b = 10.654(5)$ Å, $c = 16.234(7)$ Å, $\beta = 111.565(9)$; space group, $P2_1$; *R*-Factor, 4.97% (reported, 5.20% [17]). The same crystals were obtained from a H_2O/EtOH 6:1 soln.

3. *Computational Details.* The geometry of the systems has been optimized at the B3LYP [36][37]/6-311++G(d,p) [38] computational level. According to the calculations, the molecules and complexes correspond to the energy minima ($\lambda = 0$, where λ is the number of negative eigenvalues of the *Hessian* matrix for a given stationary point) on the potential energy surfaces (PESs). All the calculations were performed with the Gaussian-09 program [39]. The theoretical absolute shieldings (σ [ppm]) [40] were calculated using the GIAO method [41][42] on the B3LYP/6–311++G(d,p) geometries. A set of empirical equations were used to transform absolute shieldings (σ [ppm]) calculated for the molecules in the gas phase to chemical shifts (δ [ppm]) determined in soln. or in the solid state [43][44]. The same geometries have been used for the calculation of the spin-spin indirect coupling constant at the B3LYP/6-311++G(d,p) level with the GIAO method. The optimization of the complex depicted in *Fig. 4* at the M05-2X/6-31+G(d) level required 50 d (49 d 15 h 34 min 7.5 s) of CPU (central processing unit) in the computer of the *CTI* (*CSIC*).

4. *NMR Experiments Performed for Compound* **1**. ^{1}H-, ^{13}C-, and ^{15}N-NMR spectra were recorded at 298 K, using $CDCl_3$ as the solvent, on a *Varian SYSTEM 500* NMR spectrometer equipped with a 5-mm HCN cold probe, operating at 499.81 (^{1}H), 125.69 (^{13}C), and 50.65 MHz (^{15}N). ^{1}H and ^{13}C chemical shifts are reported in ppm from Me_4Si and ^{15}N chemical shifts from $MeNO_2$. ^{1}H- and ^{13}C-NMR recordings were performed using standard *Varian* pulse sequences, with digital resolutions of 0.1–0.3 Hz. ^{15}N Chemical shifts were deduced from the 2D ^{1}H,^{15}N-gHMBC experiment, with a digital resolution of 152 Hz/pt for the ^{15}N dimension.

5. *NMR Simulations.* All chemical shifts and couplings constants for compound **1** were obtained from the experimental ^{1}H-NMR spectrum. Chemical shifts and coupling constants, determined for the saturated fragment (CH_2(5)–CH_2(6)–CH(7)–NH), were then submitted (negative values for the geminal couplings and positive values for the vicinal couplings) to a spectral simulation and optimization program (gNMR5.0, IvorySoft, UK) [45], providing a complete set of optimized values by comparing experimental with simulated spectra.

6. *Discrimination Experiments Using (*S,S*)-ABTE.* 7 mg (1.8×10^{-5} mol) of (±)-**1** were dissolved in 0.6 ml of $CDCl_3$ (99.8% deuterated) and the spectrum was recorded at 600 MHz on a *Bruker Avance* spectrometer. The *Fourier transform* was carried out with the usual parameters, and the resolution was increased by mean of a Gaussian treatment of the FID. A COSY spectrum was obtained from this soln. Then, 9.1 mg (2.4×10^{-5} mol) of (*S*,*S*)-ABTE (=α,α'-bis(trifluoromethyl)anthracene-9,10-dimethanol) were added (ratio ABTE/colchicine 1.33), and the spectrum was recorded under identical conditions. In these experiments, the signals corresponding to ABTE were broad due to slow rotation about the exocyclic C–C bonds. To identify the (*S*)-enantiomer (natural) of colchicine was added in four portions, each time 0.6 mg. The best results were obtained after the third addition. For the ^{13}C- and ^{15}N-NMR experiments, the cryosonde of the *Bruker Avance* 500 MHz instrument was used.

7. *CPMAS-NMR Experiments.* ^{13}C- (100.73 MHz) and ^{15}N- (40.60 MHz) CPMAS-NMR spectra were recorded on a *Bruker WB 400* spectrometer at 300 K using a 4-mm DVT probehead and a 4-mm diameter cylindrical zirconia rotor with Kel-F end-caps. The non-quaternary suppression (NQS) technique to observe only the quaternary C-atoms was employed [46]. ^{13}C-NMR Spectra were originally referenced to a glycine sample, and then the chemical shifts were recalculated with reference to Me_4Si (for the C=O C-atom, δ (glycine) 176.1 ppm), and ^{15}N spectra were referenced to $^{15}NH_4Cl$ and then converted to $MeNO_2$ scale using the relationship: δ (^{15}N)($MeNO_2$) = δ (^{15}N)(NH_4Cl) – 338.1 ppm.

8. *IR and VCD Experiments.* The Far-IR spectrum of colchicine samples in the solid phase was recorded using a *Bruker Vertex 70* in the 700–25-cm^{-1} region, with a resolution of 4 cm^{-1} and 200 scans,

and the Pt ATR accessory (single reflection diamond ATR accessory) and the silicon beamsplitter for the far-IR region.

The *Raman* spectra of colchicine samples were recorded with a *MultiRAM Stand Alone* FT-*Raman* spectrometer, equipped with an Nd:YAG laser (excitation line at 1064 nm) and a Ge detector cooled at liquid N_2 temp. The spectra were recorded using a standard solid support with a resolution of 1 cm^{-1} and 200 scans.

The VCD spectra of colchicine samples in the $CHCl_3$ solns. and in the fluorolube/nujol mulls were recorded with a *JASCO FVS-4000* FT-IR spectrometer, equipped with a *MCTV* (2000–900 cm^{-1}) detector. A few mg of colchicine were dissolved in $CHCl_3$ or mixed with fluorolube or nujol mineral oils to obtain suitable mulls. Special attention is required when working with solid samples for CD spectroscopy [47]. In fact, we have recorded the spectra of the mulls in several positions by rotating the sample around both the beam propagation axes (90 and 180°) and that perpendicular to it (180°) to obtain the true VCD peaks and to ensure the absence of artifacts in the VCD spectra. All spectra were recorded using a standard cell equipped with BaF_2 windows, with a resolution of 4 cm^{-1}, path lengths between 6 and 50 μ (for solution spectra), and 4000 scans. Concerning the baseline correction, we have subtracted the $CHCl_3$, nujol and/or fluorolube signals from the VCD spectra.

REFERENCES

[1] K. C. Nicolaou, R. A. Valiulin, J. K. Pokorski, V. Chang, J. S. Chen, *Bioorg. Med. Chem. Lett*. **2012**, *22*, 3776.
[2] Y. B. Malysheva, S. Combes, D. Allegro, V. Peyrot, P. Knochel, A. E. Gavryushin, A. Y. Fedorov, *Bioorg. Med. Chem*. **2012**, *20*, 4271.
[3] T. Sarkar, T. L. Nguyen, Z.-W. Su, J. Hao, R. Bai, R. Gussio, S. X. Qiu, E. Hamel, *Biochem. Pharmacol*. **2012**, *84*, 444.
[4] N. Sitnikov, J. Velder, L. Abodo, N. Cuvelier, J. Neudörfl, A. Prokop, G. Krause, A. Y. Fedorov, H.-G. Schmalz, *Chem. – Eur. J.* **2012**, *18*, 12096.
[5] M. Sorkin, *Helv. Chim. Acta* **1946**, *29*, 246.
[6] M. V. King, *Acta Crystallogr.* **1952**, *5*, 437.
[7] A. Bladé-Font, *Tetrahedron Lett*. **1977**, *18*, 2977.
[8] R. Dumont, A. Brossi, J. V. Silverton, *J. Org. Chem*. **1986**, *51*, 2515.
[9] M. Cavazza, M. Zandomeneghi, F. Pietra, *Tetrahedron Lett*. **2000**, *41*, 9129.
[10] F. Pietra, *J. Phys. Org. Chem*. **2007**, *20*, 1102.
[11] A. Bladé-Font, R. Muller, J. Elguero, R. Faure, E. J. Vincent, *Chem. Lett*. **1979**, 233.
[12] J. Elguero, R. N. Muller, A. Bladé-Font, R. Faure, E. J. Vincent, *Bull. Soc. Chim. Belg*. **1980**, *89*, 193.
[13] C. D. Hufford, H.-G. Capraro, A. Brossi, *Helv. Chim. Acta* **1980**, *63*, 50.
[14] D. Meksuriyen, L.-J. Lin, G. A. Cordell, S. Mukhopadhyay, S. K. Banerjee, *J. Nat. Prod*. **1988**, *51*, 88.
[15] H.-P. He, F.-C. Liu, L. Hu, H.-Y. Zhu, *Acta Bot. Yunnanica* **1999**, *21*, 364.
[16] F. H. Allen, *Acta Crystallogr., Sect. B* **2002**, *58*, 380; F. H. Allen, W. D. S. Motherwell, *Acta Crystallogr., Sect. B* **2002**, *58*, 407; CSD version 5.32, update Feb. 2011. http://www.ccdc.cam.ac.uk.
[17] L. Lessinger, T. N. Margulis, *Acta Crystallogr., Sect. B* **1978**, *34*, 578.
[18] L. Y. Izotova, K. M. Beketov, B. T. Ibragimov, M. K. Yusupov, *J. Inclusion Phenom. Mol. Recognit. Chem.* **1997**, *28*, 33.
[19] H. W. Detrich, R. C. Williams, T. L. Macdonald, L. Wilson, D. Puett, *Biochemistry* **1981**, *20*, 5999.
[20] C. Ghatak, V. G. Rao, R. Pramanik, S. Sarkar, N. Sarkar, *J. Phys. Chem. B* **2011**, *115*, 6644.
[21] C. A. G. Haasnoot, F. A. A. M. de Leeuw, C. Altona, *Tetrahedron* **1980**, *36*, 2783.
[22] S. Ludvigsen, K. V. Andersen, F. M. Poulsen, *J. Mol. Biol*. **1991**, *217*, 731.
[23] See http://www.stenutz.eu/conf/karplus.html
[24] M. Pomares, F. Sánchez-Ferrando, A. Virgili, A. Alvarez-Larena, J. F. Piniella, *J. Org. Chem*. **2002**, *67*, 753.
[25] J. Comelles, C. Estivill, M. Moreno-Mañas, A. Virgili, A. Vallribera, *Tetrahedron* **2004**, *60*, 11541.

[26] J. Comelles, A. Pericas, M. Moreno-Mañas, A. Vallribera, G. Drudis-Solé, A. Lledos, T. Parella, A. Roglans, S. García-Granda, L. Roces-Fernández, *J. Org. Chem*. **2007**, *72*, 2077.
[27] R. J. Abraham, J. J. Byrne, L. Griffiths, M. Perez, *Magn. Reson. Chem*. **2006**, *44*, 491.
[28] Y. Zhao, N. E. Schultz, D. G. Truhlar, *J. Chem. Theory Comput*. **2006**, *2*, 364; Y. Zhao, D. G. Truhlar, *J. Chem. Theory Comput*. **2008**, *4*, 1849.
[29] G. P. A. Yap, R. M. Claramunt, C. López, M. A. García, C. Pérez-Medina, I. Alkorta, J. Elguero, *J. Mol. Struct*. **2010**, *965*, 74.
[30] H. Cano, C. Foces-Foces, J. Elguero, *Acta Crystallogr., Sect. C* **1988**, *44*, 919.
[31] J. M. Bijvoet, A. F. Peerdeman, A. J. Van Bommel, *Nature* **1951**, *168*, 271; S. Ramasehan, S. C. Abrahams, 'Anomalous Scattering', Munksgaard, Copenhagen, DK, 1975.
[32] S. Graus, R. M. Tejedor, S. Uriel, J. L. Serrano, I. Alkorta, J. Elguero, *J. Am. Chem. Soc.* **2010**, *132*, 7862.
[33] I. Alkorta, J. Elguero, C. Roussel, *Tetrahedron: Asymmetry* **2011**, *22*, 1180.
[34] F. Partal Ureña, J. R. Avilés Moreno, J. J. López González, *J. Phys. Chem. A* **2008**, *112*, 7887; J. R. Avilés Moreno, F. Partal Ureña, J. J. López González, *Phys. Chem. Chem. Phys.* **2009**, *11*, 2459; J. R. Avilés Moreno, M. M. Quesada Moreno, F. Partal Ureña, J. J. López González, *Tetrahedron: Asymmetry* **2012**, *23*, 1084; T. R. Huet, J. R. Avilés Moreno, O. Pirali, M. Tudorie, F. Partal Ureña, J. J. López González, *J. Quant. Spectrosc.* **2012**, *113*, 1261; F. Partal Ureña, J. R. Avilés Moreno, J. J. López González, *Chirality* **2010**, *22*, E123; J. R. Avilés Moreno, J. J. López González, F. Partal Ureña, F. Vera, M. B. Ros, T. Sierra, *J. Phys. Chem. B* **2012**, *116*, 5090; J. J. L. González, F. P. Ureña, J. R. A. Moreno, I. Mata, E. Molins, R. M. Claramunt, C. López, I. Alkorta, J. Elguero, *New J. Chem.* **2012**, *36*, 749.
[35] NIST Standard Reference Database 101, Computational Chemistry Comparison and Benchmark DataBase: http://cccbdb.nist.gov/vibscalejust.asp.
[36] A. D. Becke, *J. Chem. Phys.* **1993**, *98*, 5648.
[37] C. T. Lee, W. T. Yang, R. G. Parr, *Phys. Rev. B* **1988**, *37*, 785.
[38] M. J. Frisch, J. A. Pople, J. S. Binkley, *J. Chem. Phys.* **1984**, *80*, 3265.
[39] M. J. Frisch, G. W. Trucks, H. B. Schlegel, G. E. Scuseria, M. A. Robb, J. R. Cheeseman, G. Scalmani, V. Barone, B. Mennucci, G. A. Petersson, H. Nakatsuji, M. Caricato, X. Li, H. P. Hratchian, A. F. Izmaylov, J. Bloino, G. Zheng, J. L. Sonnenberg, M. Hada, M. Ehara, K. Toyota, R. Fukuda, J. Hasegawa, M. Ishida, T. Nakajima, Y. Honda, O. Kitao, H. Nakai, T. Vreven, J. A. Montgomery Jr., J. E. Peralta, F. Ogliaro, M. Bearpark, J. J. Heyd, E. Brothers, K. N. Kudin, V. N. Staroverov, R. Kobayashi, J. Normand, K. Raghavachari, A. Rendell, J. C. Burant, S. S. Iyengar, J. Tomasi, M. Cossi, N. Rega, J. M. Millam, M. Klene, J. E. Knox, J. B. Cross, V. Bakken, C. Adamo, J. Jaramillo, R. Gomperts, R. E. Stratmann, O. Yazyev, A. J. Austin, R. Gaussian, Inc.: Wallingford CT, 2009.
[40] P. v. R. Schleyer, C. Maerker, A. Dransfeld, H. Jiao, N. J. R. v. E. Hommes, *J. Am. Chem. Soc.* **1996**, *118*, 6317.
[41] R. Ditchfield, *Mol. Phys.* **1974**, *27*, 789.
[42] F. London, *J. Phys. Radium* **1937**, *8*, 397.
[43] A. M. S. Silva, R. M. S. Sousa, M. L. Jimeno, F. Blanco, I. Alkorta, J. Elguero, *Magn. Reson. Chem*. **2008**, *46*, 859.
[44] F. Blanco, I. Alkorta, J. Elguero, *Magn. Reson. Chem.* **2007**, *45*, 797.
[45] gNMR5.0, IvorySoft, AmorWay, Letchworth, Herts. SG61ZA, UK, 2004.
[46] S. Berger, S. Braun, '200 and more NMR Experiments', Wiley-VCH, Weinheim, 2004.
[47] R. Kuroda, T. Harada, Y. Shindo, *Rev. Sci. Instrum.* **2004**, *72*, 3802; C. Merten, T. Kowalik, A. Hartwig, *Appl. Spectrosc.* **2008**, *62*, 901; T. Buffeteau, F. Lagugné-Labarthet, C. Sourisseau, *Appl. Spectrosc.* **2005**, *59*, 732.

Received November 6, 2013